
PuriDefense: Randomized Local Implicit Adversarial Purification for Defending Black-box Query-based Attacks

Ping Guo¹ Zhiyuan Yang¹ Xi Lin¹ Qingchuan Zhao¹ Qingfu Zhang¹

Abstract

Black-box query-based attacks constitute significant threats to Machine Learning as a Service (MLaaS) systems since they can generate adversarial examples without accessing the target model’s architecture and parameters. Traditional defense mechanisms, such as adversarial training, gradient masking, and input transformations, either impose substantial computational costs or compromise the test accuracy of non-adversarial inputs. To address these challenges, we propose an efficient defense mechanism, PuriDefense, that employs random patch-wise purifications with an ensemble of lightweight purification models at a low level of inference cost. These models leverage the local implicit function and rebuild the natural image manifold. Our theoretical analysis suggests that this approach slows down the convergence of query-based attacks by incorporating randomness into purifications. Extensive experiments on CIFAR-10 and ImageNet validate the effectiveness of our proposed purifier-based defense mechanism, demonstrating significant improvements in robustness against query-based attacks.

1. Introduction

Deep neural networks (*DNNs*), while presenting remarkable performance across various applications, are mostly leaning to become subject to *adversarial attacks*, where even slight perturbations to the inputs can severely compromise their predictions (Szegedy et al., 2014). This notorious vulnerability significantly challenges the inherent robustness of *DNNs* and could even make the situation much worse when it comes to security-critical scenarios, such as facial recognition (Dong et al., 2019) and autonomous driving (Cao et al., 2019). Accordingly, attackers have devised both *white-box attacks* if having full access to the *DNN*

model and *black-box attacks* in case the model is inaccessible. While black-box attacks appear to be more challenging, it is often considered a more realistic threat model, and its state-of-the-art (SOTA) could leverage a limited number of queries to achieve high successful rates against closed-source commercial platforms, *i.e.* Clarifai (Clarifai, 2022) and Google Cloud Vision API (Google, 2022), presenting a disconcerting situation (Liu et al., 2017).

Defending black-box query-based attacks in real-world large-scale Machine-Learning-as-a-Service (*MLaaS*) systems calls for an extremely low extra inference cost. This is because business companies, such as Facebook, handle millions of image queries daily and thereby increase the extra cost for defense a million-fold (VentureBeat, 2022). This issue prohibits testing time defenses to run multiple inferences to achieve *certified robustness* (Cohen et al., 2019; Salman et al., 2020b). Moreover, training time defenses, *i.e.* retraining the *DNNs* with large datasets to enhance their robustness against adversarial examples (*e.g.* *adversarial training* (Madry et al., 2018) and *gradient masking* (Tramèr et al., 2018)), impose substantial economic and computational costs attributed to the heavy training expense. Therefore, there is a critical need for a lightweight yet effective strategy to perform adversarial purifications to enable low inference cost for achieving robustness.

Given the aforementioned challenges, recent research efforts have been devoted to either eliminating or disturbing adversarial perturbations prior to the forwarding of the query image to the classifier. Nevertheless, the existing methods that include both heuristic transformations and neural network-based adversarial purification models have certain limitations in removing adversarial perturbations. While heuristic transformation methods cause minimal impact on cost, they merely disrupt adversarial perturbations and often negatively impact the testing accuracy of non-adversarial inputs (Xu et al., 2018; Qin et al., 2021). Moreover, neural network-based purifications aiming to completely eradicate adversarial perturbations can even exceed the computational burden of the classifier itself (Carlini et al., 2023). Consequently, there have been no effective defense mechanisms that can achieve both high robustness and low computational cost against black-box query-based attacks.

¹Department of Computer Science, City University of Hong Kong, Hong Kong. Correspondence to: Ping Guo <pingguo5-c@my.cityu.edu.hk>.

In this study, we present PuriDefense, a novel random patch-wise image purification mechanism that leverages local implicit functions to enhance the robustness of classifiers against query-based attacks. Local implicit functions, initially developed for super-resolution applications (Lim et al., 2017; Zhang et al., 2018), have shown potential in efficiently mitigating white-box attacks (Ho & Vasconcelos, 2022). Nonetheless, our empirical analysis indicates that a naively integrated local implicit function with a classifier yields a system vulnerable to query-based attacks, achieving only a 5.1% robust accuracy on the ImageNet dataset in potent attack scenarios. Our theoretical examination attributes this vulnerability to the absence of inherent randomness in the purification process.

While randomness can be incorporated through a collection of diverse purifiers (Ho & Vasconcelos, 2022), this approach linearly increases the inference cost. In contrast, PuriDefense enhances diversity without escalating inference costs, utilizing a pool of varied purifiers and assigning them to local image patches randomly. Our analysis confirms that with a broader spectrum of purifiers, the system exhibits higher resilience and effectively slows down the convergence of the query-based attacks.

Our contributions are summarized as follows:

- We propose a novel defense mechanism using the local implicit function to randomly purify adversarial image patches using multiple purification models while maintaining the inference cost of a single model. Our work is the first to extend the local implicit function to defend against query-based attacks.
- We present a theoretical analysis illustrating the defense mechanism’s effectiveness based on the convergence of black-box attacks. Our theoretical analysis suggests the robustness of our system escalates with the number of purifiers in the purifier pool.
- Our theoretical investigation further reveals the susceptibilities of *deterministic purifications*’ to query-based attacks and quantifies the enhanced robustness achieved by integrating randomness into any preprocessor-based defense strategy.
- We validate our method’s defense capabilities through comprehensive experiments conducted on the CIFAR-10 and ImageNet datasets, specifically targeting SOTA query-based attacks.

2. Related Work

Query-based Attacks. Query-based attacks, continually querying the models to generate adversarial examples, are

categorized as either *score-based* or *decision-based*, based on their access to confidence scores or labels, respectively.

Score-based attacks treat the MLaaS model, encompassing its pre-processors, the primary model, and post-processors, as an opaque entity. The typical objective function in this scenario is the marginal loss of confidence scores, illustrated in Equation (1). To address the challenge of minimizing this loss, methods such as *gradient estimation* and *random search* are employed. Ilyas et al. (2018) developed the pioneering limited-query score-based method, utilizing Natural Evolutionary Strategies (NES) for gradient estimation. This sparked a flurry of subsequent studies focusing on gradient estimation, methods like ZO-SGD (Liu et al., 2019) and SignHunter (Al-Dujaili & O’Reilly, 2020). The forefront of score-based attack methods is represented by the Square attack (Andriushchenko et al., 2020), which employs random search via localized square patch modifications and is often referenced as an important benchmark in model robustness assessments (Croce et al., 2021). Other algorithms that employ random search, such as SimBA (Guo et al., 2019), exist but do not achieve the effectiveness of the Square attack.

With respect to decision-based attacks, when confidence scores are not available, the available label information is used instead. Ilyas et al. (2018) also pioneered work in this area, employing NES to optimize a heuristic proxy function with a limited number of queries. The gradient estimation method for decision-based attacks evolves to be more efficient by forming new optimization problems (e.g., OPT (Cheng et al., 2019)), and focusing on the gradient’s sign rather than its magnitude (e.g., Sign-OPT (Cheng et al., 2020) and HopSkipJump (Chen et al., 2020)). While direct search used in Boundary Attack (Brendel et al., 2018) is the first decision-based attack, the HopSkipJump Attack is currently recognized as the most advanced attack.

Adversarial Purification. The recent surge in the implementation of testing-time defenses, primarily for adversarial purification to enhance model robustness, is noteworthy. Yoon et al. (2021) proposes the use of a score-based generative model to mitigate adversarial perturbations. Meanwhile, Mao et al. (2021) employs self-supervised learning techniques, such as contrastive loss, to purify images. Following the success of diffusion models, purifications have been utilized to establish certified robustness for image classifiers (Nie et al., 2022; Carlini et al., 2023). However, the complexity and vast number of parameters of diffusion models result in significantly reduced inference speeds of the classification systems.

The recent literature also notes the introduction of the local implicit function model as a defense against white-box attacks (Ho & Vasconcelos, 2022). Nonetheless, this approach has limitations, being trained only on white-box attacks and lacking theoretical guarantees for resisting black-box at-

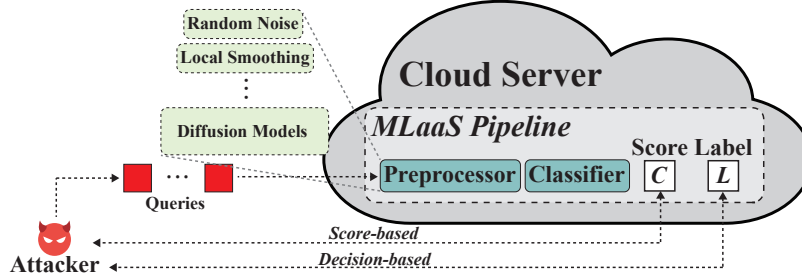


Figure 1. An illustration of the MLaaS system with preprocessor-based defense mechanisms under attack. The attackers can query the model with input \mathbf{x} and get the returned information $\mathcal{M}(\mathbf{x})$ which can be the confidence scores or the predicted label.

tacks. In contrast, our study restructures the network to omit multi-resolution support and accelerates the inference time by a factor of four in the implementation level. Furthermore, our defense mechanism design ensures that the inference speed remains constant as the number of purifier models increases, with a theoretical guarantee for resisting black-box attacks. Further information on general defense mechanisms is available for interested readers in Appendix A.

3. Preliminaries

3.1. Threat Model

In the context of black-box query-based attacks, our threat model assumes that attackers possess have a limited comprehension of the target model. The interaction with the model, usually deployed on cloud servers, is confined to submitting queries and obtaining outputs as confidence scores or classifications. Attackers are deprived of deeper understanding of the model’s internal mechanisms or the datasets employed. Figure 1 depicts the MLaaS system under attack

3.2. Query-based Attacks

3.2.1. SCORE-BASED ATTACKS

Consider a classifier $\mathcal{M} : \mathcal{X} \rightarrow \mathcal{Y}$ deployed on a cloud server, where \mathcal{X} denotes the input space and \mathcal{Y} represents the output space. Attackers may query the model using an input $\mathbf{x} \in \mathcal{X}$ and receive the corresponding output $\mathcal{M}(\mathbf{x}) \in \mathcal{Y}$. When the model furnishes its output, typically as a confidence score, directly to the attackers, this situation typifies a score-based attack.

In this context, attackers craft an adversarial example \mathbf{x}_{adv} using the original example \mathbf{x} and its corresponding true label y . Their goal is to address the optimization challenge below, which is necessary to conduct an untargeted attack:

$$\min_{\mathbf{x}_{adv} \in \mathcal{N}_R(\mathbf{x})} f(\mathbf{x}_{adv}), \quad (1)$$

$$f(\mathbf{x}_{adv}) = \mathcal{M}_y(\mathbf{x}_{adv}) - \max_{j \neq y} \mathcal{M}_j(\mathbf{x}_{adv}).$$

Here, $\mathcal{N}_R(\mathbf{x}) = \{\mathbf{x}' \mid \|\mathbf{x}' - \mathbf{x}\|_p \leq R\}$ represents the ℓ_p -norm ball centered at \mathbf{x} . For targeted attacks, the variable

j is specified as the designated target label, in contrast to being the index associated with the highest confidence score that is not the true label. An attack is considered successful if it results in the objective function falling below zero.

In white-box attacks, the projected gradient descent algorithm is employed; however, in a black-box setting, attackers lack access to gradient details. Consequently, black-box methods typically rely on two approaches to approximate the direction of function descent: *gradient estimation* and *heuristic search*. Additional information on these techniques can be found in Appendix B.

3.2.2. DECISION-BASED ATTACKS

In decision-based attack scenarios, attackers receive only the output label from the model after querying it. In response to the noncontinuous nature of the objective function’s landscape, researchers have developed a variety of optimization problems (Cheng et al., 2019). For instance, Ilyas et al. (2018) propose using a surrogate for the objective function, while Cheng et al. (2020) and Aithal & Li (2022) innovate approaches based on geometric concepts. Furthermore, Chen et al. (2020) tackle the original optimization problem by utilizing the gradient’s sign. The principles outlined in our theoretical examination of score-based attacks are also applicable to decision-based attacks since both employ similar black-box optimization techniques.

3.3. Adversarial Purification

Adversarial purification has recently emerged as a central wave of defense against adversarial attacks, which aims to remove or disturb the adversarial perturbations via *heuristic transformations* and *purification models*. We have provided a list of widely heuristic transformations and SOTA purification models in Table 1.

Heuristic Transformations. Heuristic transformations are unaware of the adversarial perturbations and only aim to disturb the adversarial perturbations by shrinking the image space (Xu et al., 2018) or deviating the gradient estimation using random noises (Qin et al., 2021).

Table 1. List of heuristic transformations and SOTA purification models. Randomness is introduced in DISCO (Ho & Vasconcelos, 2022) by using an ensemble of DISCO models to generate features for random coordinate querying, which is of high computational cost.

Method	Randomness	Type	Inference Cost
Bit Reduction (Xu et al., 2018)	✗	Heuristic	Low
Local Smoothing (Xu et al., 2018)	✗	Heuristic	Low
JPEG Compression (Raff et al., 2019)	✗	Heuristic	Low
Random Noise (Qin et al., 2021)	✓	Heuristic	Low
Score-based Model (Yoon et al., 2021)	✓	Neural	High
DDPM (Nie et al., 2022)	✓	Neural	High
DISCO (Ho & Vasconcelos, 2022)	✗ / ✓	Neural	Median / High
PuriDefense (Ours)	✓	Neural	Median

Purification Models. Advanced models for purification have been developed to eliminate adversarial perturbations. Notably, the score-based generative model (Yoon et al., 2021) and DDPM (Nie et al., 2022), and local implicit purification models like DISCO (Ho & Vasconcelos, 2022). However, of these, only the local implicit purification demonstrates a moderate inference cost necessary for practical, real-world applications.

With defense mechanisms deployed as pre-processors in the MLaaS system as shown in Figure 1, the attackers need to break the whole MLaaS pipeline to mount a successful attack. Although randomness has been identified as crucial in enhancing system robustness (Raff et al., 2019; Sitawarin et al., 2022), the naive implementation of randomness through the ensemble of multiple purifiers, such as DISCO, incurs a linear increase in the inference cost.

4. Randomized Local Implicit Purification

4.1. Our Motivation

While purification models can process adversarial images, our research, detailed in our theoretical analysis (section 4.5) and substantiated in the experiments (section 5.2), indicates that a *single deterministic purifier* is insufficient for enhancing the robustness of a system against query-based attacks and may inadvertently introduce new vulnerabilities. While a direct ensemble of purifiers may seem effective in principle, the consequent linear increase in inference cost proportional to the number of purifiers renders the approach impractical for real-world deployment.

In response to this challenge, we propose a novel random patch-wise purification algorithm, PuriDefense, that capitalizes on a pool of purifiers to counter query-based attacks efficiently. PuriDefense employs multiple end-to-end purification models that utilize a local implicit function to process input images at any scale. Our theoretical findings demonstrate that the enhanced robustness of PuriDefense scales with the number of purifiers used. Most importantly, it maintains a consistent inference cost regardless of the

number of purifiers, thereby offering a viable solution for deployment in practical settings.

4.2. Image Purification via Local Implicit Function

Consider a purification model $m(x) : \mathcal{X} \rightarrow \mathcal{X}$ designed to project adversarial images back onto the natural images manifold. When attackers craft adversarial example x' from the original image x , randomly drawn from the natural image distribution \mathcal{D} . The purification model $m(x)$ can be refined by minimizing the following loss function:

$$\mathcal{L} = \mathbb{E}_{\mathcal{D}} \|x - m(x')\|_p + \lambda \mathbb{E}_{\mathcal{D}} \|x - m(x)\|_p, \quad (2)$$

where the parameter λ balances the two components of the loss. A larger λ signifies a greater emphasis on fidelity to unaltered images. In practice, the second term is often disregarded ($\lambda = 0$). The ℓ_1 -norm ($p = 1$) is commonly utilized for its pixel-level accuracy in quantifying the discrepancy between the original and the purified image.

Local Implicit Purification Model. To project the images suffering from adversarial perturbations onto the natural image manifold, we leverage a local implicit function designed to reconstruct the image area surrounding the perturbed pixels. Our model adopts an encoder-decoder framework. In this process, image patches are first encoded into a high-dimensional feature space. Subsequently, the decoder harnesses this space to restore the original RGB values of the pixels. This reconstruction is performed concurrently for all pixels within a patch, as depicted in Figure 2, which also details the architecture of our model.

Efficient Design. In contrast to the initial strategy of utilizing a local implicit function to defend against white-box attacks (Ho & Vasconcelos, 2022), our design removes the multi-scale support by dispensing with positional encoding and local ensemble inference. This simplification yields a fourfold acceleration in inference time at the implementation level. A comprehensive elucidation of this accelerated implementation is provided in Appendix D.1.

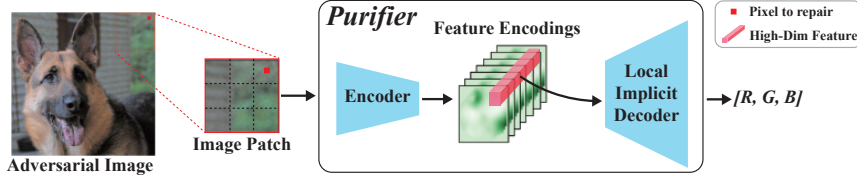


Figure 2. An illustration of repairing a pixel within an image patch with our end-to-end purification model. The encoder diffuses nearby information of the pixel into its high-dimensional feature. Then the decoder reconstructs its RGB value with respect to this feature information. Note that the inference of pixels within one image patch can be performed in parallel.

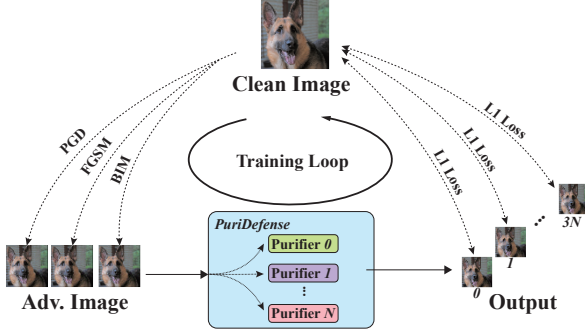


Figure 3. The training process of PuriDefense. Firstly, different adversarial images are generated using white-box attack algorithms. Then, we train every purifier inside PuriDefense with these adversarial images and original images under ℓ_1 loss.

4.3. Training Purifiers in PuriDefense

In PuriDefense, our strategy entails implementing a series of purification models to establish a varied ensemble for randomized patch-wise purification. Consequently, we have developed training protocols that enable the simultaneous training of diverse models, each with a distinct architecture. The procedural flow of our training methodology is delineated in Figure 3.

During the training process, adversarial samples generated by applying three advanced white-box attack techniques—PGD (Madry et al., 2018), FGSM (Goodfellow et al., 2015), and BIM (Kurakin et al., 2017b)—to non-protected models. The purifiers then cleanse the perturbed inputs. Next, the purified samples and original images are used to calculate the training loss as per Equation (2). A back-propagation algorithm subsequently optimizes all the purifiers in PuriDefense. Additional information like regarding the non-defended models and the purifiers’ architecture can be found in Appendix D.2.

4.4. Random Patch-wise Purification.

Random patch-wise purification constitutes the core of our defensive approach, designed to introduce randomness into the purification process, which is critical for defending against query-based attacks. It maintains the computational cost of employing multiple purifiers at a level that is equivalent to that of a single model, which is crucial for real-world deployment, as opposed to the current approach (ensem-

ble) that escalates the inference cost proportionally to the number of purifiers employed (Ho & Vasconcelos, 2022).

Our method encodes image patches using randomly selected purifiers from the purifier pool and subsequently merges their outputs to construct the final feature representation, in contrast to previous techniques that necessitate full-image encoding followed by random feature selection. As depicted in Figure 4, this approach—although employing potentially deterministic purifiers—ensures randomness by the unpredictable selection of both the purifiers for performing purifications. Such a strategy significantly augments the diversity of purifiers while maintaining reasonable inference cost.

4.5. Theoretical Analysis for Gradient-based Attacks

Assume we have $K + 1$ purifiers $\{\mathbf{m}_0, \dots, \mathbf{m}_K\}$, the output of the new black-box system containing the i -th purifier is defined as $F^{(i)}(\mathbf{x}) = f(\mathbf{m}_i(\mathbf{x}))$. Without loss of generality, we now perform analysis on breaking the system of the purifier \mathbf{m}_0 , denoted as $F(\mathbf{x}) = f(\mathbf{m}_0(\mathbf{x}))$. Our following analysis utilizes the ℓ_2 -norm as the distance metric, which is the most commonly used norm for measuring the distance between two images.

Suppose the index of two independently drawn purifiers in our defense are k_1 and k_2 , the attacker approximate the gradient of the function $F(\mathbf{x})$ with the following estimator:

$$G_{\mu,K} = \frac{f(\mathbf{m}_{k_1}(\mathbf{x} + \mu\mathbf{u})) - f(\mathbf{m}_{k_2}(\mathbf{x}))}{\mu}\mathbf{u}, \quad (3)$$

where \mathbf{u} is a standard Gaussian noise vector. The above gradient estimator provides an *unbiased* estimation of the gradient of the function:

$$F_{\mu,K}(\mathbf{x}) = \frac{1}{K+1} \sum_{k=0}^K f_{\mu}(\mathbf{m}_k(\mathbf{x})), \quad (4)$$

where f_{μ} is the gaussian smoothing function of f . The detailed definition of the gaussian smoothing function is included in Appendix E.1. The convergence of the black-box attack is moving towards an *averaged* optimal point of the functions $F^{(i)}$ formed with different purifiers \mathbf{m}_i .

Assumptions. For the original function $f(\mathbf{x})$, we have Assumption 1 and Assumption 2. With regards to the purifiers, we assume each output dimension (every pixel in



Figure 4. An illustration of the encoding process of ensemble method (Ho & Vasconcelos, 2022) and our method. **Ensemble:** Ensemble method first encodes the image into multiple high-dimension features and then randomly combines their pieces to form the final feature representation. **Random Patch-wise:** Our method split the images into patches, forward them to randomly selected encoders, and use the output combination as the final feature representation.

one channel) of their output also has the property in Assumption 1 and Assumption 2. Then, we denote $L_0(\mathbf{m}) = \max_i L_0(m_i)$ and $L_1(\mathbf{m}) = \max_i L_1(m_i)$, where m_i is the i -th dimension of the output of the purifier \mathbf{m} .

Assumption 1. $f(\mathbf{x})$ is Lipschitz-continuous, i.e., $|f(\mathbf{y}) - f(\mathbf{x})| \leq L_0(f)\|\mathbf{y} - \mathbf{x}\|$.

Assumption 2. $f(\mathbf{x})$ is continuous and differentiable, and $\nabla f(\mathbf{x})$ is Lipschitz-continuous, i.e., $\|\nabla f(\mathbf{y}) - \nabla f(\mathbf{x})\| \leq L_1(f)\|\mathbf{y} - \mathbf{x}\|$.

Furthermore, we bound the diversity of the purifiers using the following property:

$$\|\mathbf{m}_i(\mathbf{x}) - \mathbf{m}_j(\mathbf{x})\| < \nu, \quad \forall i, j \in \{0, \dots, K-1\} \quad (5)$$

We cannot directly measure ν , but we intuitively associate it with the number of purifiers. **The larger the number of purifiers, the larger ν is.**

Notations. We denote the sequence of standard Gaussian noises used to approximate the gradient as $\mathbf{U}_t = \{\mathbf{u}_0, \dots, \mathbf{u}_t\}$, with t to be the update step. The purifier index sequence is denoted as $\mathbf{k}_t = \{k_0, \dots, k_t\}$. The generated query sequence is denoted as $\{\mathbf{x}_0, \mathbf{x}_1, \dots, \mathbf{x}_Q\}$. $d = |\mathcal{X}|$ as the input dimension.

With the above definitions and assumptions, we have Theorem 1 for the convergence of the gradient-based attacks. The detailed proof is included in Appendix E.2.

Theorem 1. Under Assumption 1, for any $Q \geq 0$, consider a sequence $\{\mathbf{x}_t\}_{t=0}^Q$ generated using the update rule of gradient-based score-based attacks, with constant step size, i.e., $\eta = \sqrt{\frac{2R\epsilon}{(Q+1)L_0(f)^3 d^2}} \cdot \sqrt{\frac{1}{L_0(\mathbf{m}_0)\gamma(\mathbf{m}_0, \nu)}}$, with $\gamma(\mathbf{m}_0, \nu) = \frac{4\nu^2}{\mu^2} + \frac{4\nu}{\mu} L_0(\mathbf{m}_0) d^{\frac{1}{2}} + L_0(\mathbf{m}_0)^2 d$. Then, the squared norm of gradient is bounded by:

$$\begin{aligned} & \frac{1}{Q+1} \sum_{t=0}^Q \mathbb{E}_{\mathbf{U}_t, \mathbf{k}_t} [\|\nabla F_{\mu, K}(\mathbf{x}_t)\|^2] \\ & \leq \sqrt{\frac{2L_0(f)^5 R d^2}{(Q+1)\epsilon}} \cdot \sqrt{\gamma(\mathbf{m}_0, \nu) L_0(\mathbf{m}_0)^3} \end{aligned} \quad (6)$$

The lower bound for the expected number of queries to bound the expected squared norm of the gradient of function

$F_{\mu, K}$ of the order δ is

$$O\left(\frac{L_0(f)^5 R d^2}{\epsilon \delta^2} \gamma(\mathbf{m}_0, \nu) L_0(\mathbf{m}_0)^3\right) \quad (7)$$

Single Deterministic Purifier. Setting ν to 0, we have $\gamma(\mathbf{m}_0, 0) L_0(\mathbf{m}_0)^2 = L_0(\mathbf{m}_0)^5$, which is the only introduced term compared to the original convergence rate (Nesterov & Spokoiny, 2017) towards $f(\mathbf{x})$. Meanwhile, the new convergence point becomes $F_{\mu}^*(\mathbf{x})$. We have the following conclusion for the convergence of the attack:

- **Influence of $L_0(\mathbf{m}_0)$:** For input transformations that shrink the image space, since their $L_0(\mathbf{m}_0) < 1$, they always allow a faster rate of attack's convergence. For neural network purifiers, the presence of this term means their vulnerabilities is introduced into the black-box system, making it hard to quantify the robustness of the system.
- **Optimal point $F_{\mu}^*(\mathbf{x})$:** By using a deterministic transformations, the optimal point of the attack is changed from f^* to $F_{\mu}^*(\mathbf{x})$. If we can inversely find an adversarial image $\mathbf{x}^* = \mathbf{m}(\mathbf{x}^*)$, the robustness of the system is not improved at all. *No current work can theoretically eliminate this issue.* This may open up a new direction for future research.

Research implications. From the above analysis, we can see that a single deterministic purifier may 1) accelerate the convergence of the attack, and 2) cannot protect the adversarial point from being exploited.

Pool of Deterministic Purifiers. The introduced term $\gamma(\mathbf{m}_0, \nu) L_0(\mathbf{m}_0)^2$ increase quadratically with ν . This along with our intuition mentioned above suggests that the robustness of the system increases with the number of purifiers. While adversarial optimal points persist, the presence of multiple optimal points under different purifiers serve as the first trial to enhance the robustness of all purification-based methods.

To validate our theoretical analysis, we conduct experiments on the test set of the CIFAR-10 dataset (Krizhevsky, 2009) with a weak non-defended ResNet-18 model (Dadalto, 2022)

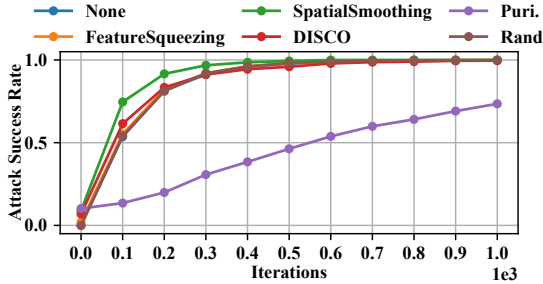


Figure 5. The convergence of the Square Attack on CIFAR-10 using different heuristic transformations and purifiers.

as the classifier. Other general settings are the same as used in our later experiments. We use the Square Attack (Andriushchenko et al., 2020) as the attack algorithm. The convergence of the attack against our model and other input transformations is shown in Figure 5. We can see a clear acceleration of the convergence of the attack with the introduction of transformations that *shrink* the image space and powerful deterministic models (DISCO) fails to improve the robustness of the system. Another validation of our theoretical analysis is shown in Figure 6 for proving the robustness of the system increases with the number of purifiers (associated with ν).

4.6. Theoretical Analysis for Gradient-free Attacks

The heuristic direction of random search becomes:

$$H_K(x) = f(m_{k_1}(x + \mu u)) - f(m_{k_2}(x + \mu u)). \quad (8)$$

Theorem 2. Under Assumption 1, using the update in Equation (8),

$$P(\text{Sign}(H(x)) \neq \text{Sign}(H_K(x))) \leq \frac{2\nu L_0(f)}{|H(x)|} \quad (9)$$

A similar increase in the robustness as Theorem 1 can be observed with the increase of ν . The detailed proof is included in Appendix E.3. This ensures the robustness of our defense against gradient-free attacks.

5. Evaluation

5.1. Experiment Settings

Datasets and Classification Models. For a comprehensive evaluation of PuriDefense, we employ two benchmark datasets for testing adversarial attacks: CIFAR-10 (Krizhevsky, 2009) and ImageNet (Deng et al., 2009). Our evaluation is conducted on two balanced subsets, which contain 1,000 and 2,000 test images randomly sampled from the CIFAR-10 test set and ImageNet validation set, respectively. These subsets are evenly distributed across the 10 classes of CIFAR-10 and 200 randomly chosen classes from ImageNet. In terms of classification models, we selected

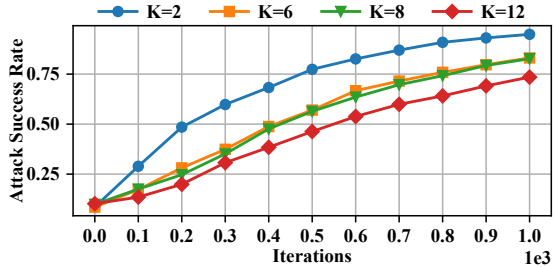


Figure 6. The convergence of the Square Attack on CIFAR-10 using with different numbers of purifiers used.

models from RobustBench (Croce et al., 2021). The details of both the standardly trained and adversarially trained models are described in Appendix C.4.

Attack and Defense Methods. We consider 5 query-based attacks for evaluation: NES (Ilyas et al., 2018), SimBA (Guo et al., 2019), Square (Andriushchenko et al., 2020), Boundary (Brendel et al., 2018), and HopSkipJump (Chen et al., 2020). Comprehensive descriptions and configurations of each attack can be found in Appendix C.2. The perturbation budget of ℓ_∞ attacks is set to 8/255 for CIFAR-10 and 4/255 for ImageNet. For ℓ_2 attacks, the perturbation budget is set to 1.0 for CIFAR-10 and 5.0 for ImageNet. For defense mechanism, adversarially trained models from (Gowal et al., 2020) are used as a strong robust baseline. Moreover, we include a deterministic purification model DISCO (Ho & Vasconcelos, 2022) and spatial smoothing (Xu et al., 2018) for direct comparison. Finally, widely used random noise defense (Qin et al., 2021) serve as a baseline for introducing randomness. The detailed settings of each defense method are described in Appendix C.3. We report the robust accuracy of each defense method against each attack with 200/2500 queries for both CIFAR-10 and ImageNet, reflecting models’ performance under mild and extreme query-based attacks.

5.2. Overall Defense Performance

Our numerical results on the effectiveness of the defense mechanisms are shown in Table 2.

Clean Accuracy. Empirical evaluations demonstrate that PuriDefense yields clean accuracy comparable to the standardly trained model. Notably, integrating PuriDefense with models trained adversarially enhances their clean accuracy at no additional cost. Further experiments offer an in-depth analysis of the variations in clean accuracy with the implementation of PuriDefense.

Failure of Deterministic Purification. As presented in Table 2, spatial smoothing accelerates the convergence of the attacks, and DISCO experiences a significant decrease in robust accuracy under 2500 queries when faced with a powerful attack (Square Attack), which is even lower

Table 2. Evaluation results of PuriDefense and other defense methods on CIFAR-10 under 5 query-based attacks. The robust accuracy under 200/2500 queries is reported. The best defense mechanism under 2500 queries are highlighted in bold and marked with gray.

Datasets	Methods	Acc.	NES(ℓ_∞)	SimBA(ℓ_2)	Square(ℓ_∞)	Boundary(ℓ_2)	HopSkipJump(ℓ_∞)
CIFAR-10 (WideResNet-28)	None	94.8	83.4/11.9	49.1/3.0	26.6/0.9	88.4/60.0	72.0/72.6
	AT (Gowal et al., 2020)	85.5	83.8/78.8	83.0/74.9	77.5/67.3	84.7/84.2	85.3/84.0
	FS (Xu et al., 2018)	76.4	50.7/7.6	42.7/5.2	5.7/0.0	70.7/39.8	64.6/62.7
	IR (Qin et al., 2021)	77.1	74.7/71.1	71.5/66.0	64.1/60.5	74.4/76.4	71.0/74.1
	DISCO (Ho & Vasconcelos, 2022)	86.3	83.0/34.7	77.7/15.7	21.0/2.1	84.1/66.0	81.0/81.7
	PuriDefense (Ours)	84.1	84.2/81.8	81.1/74.4	77.3/67.8	82.9/82.9	82.5/84.8
	PuriDefense-AT (Ours)	84.6	83.7/81.1	83.3/80.6	81.5/78.7	84.4/84.1	84.3/84.1

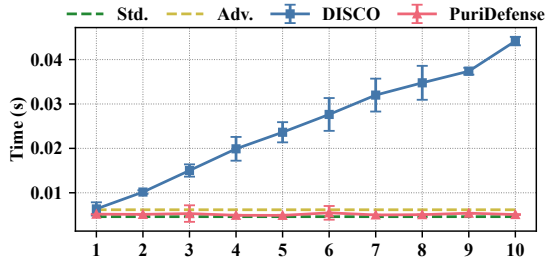


Figure 7. The inference speed of DISCO, PuriDefense, along with the standalone classifier with or without adversarial training on CIFAR-10 dataset.

than that of models without defenses. These outcomes reinforce our theoretical discourse, suggesting that deterministic transformations may inadvertently introduce additional vulnerabilities and expedite adversarial attacks. Consequently, incorporating randomness into purification processes is not only theoretically grounded but also empirically validated.

Effectiveness of PuriDefense. PuriDefense consistently attains the highest robust accuracy against various attacks on the CIFAR-10 dataset under extreme query-based attacks (2500 queries). When integrated with standardly trained model, the system reaches a robust accuracy comparable to SOTA adversarially trained models. Furthermore, PuriDefense, when combined with adversarially trained models, sets new benchmarks in robust accuracy. Its efficacy against a variety of query-based attacks demonstrates PuriDefense’s versatility as a universal defense mechanism effective against both ℓ_∞ and ℓ_2 attacks.

5.3. Inference Speedup

Our mechanism achieves a constant inference cost, which we verify in this section. The inference speed of DISCO and PuriDefense was tested on a workstation equipped with a single NVIDIA RTX 4090 GPU. We set the batch size to 1 and varied the number of purifiers from 1 to 10. To minimize the influence of data transmission delay, we measured the time of the last 900 inferences out of a total of 1000 iterations. To ensure fair comparison, both DISCO and PuriDefense utilized identical encoders and decoders; therefore, differences in inference stem solely from their respective methods. We employed the same models, standardized and adversarially

trained, as established in section 5 for baseline comparison.

Results. For CIFAR-10, the outcomes are presented in Figure 7. Additional results for ImageNet are provided in Appendix C.1, corroborating the consistency of the findings. Unlike our method, which sustains a steady inference cost regardless of the number of purifiers, DISCO’s cost escalates almost linearly. PuriDefense maintains its cost at the baseline classifier level, demonstrating its advantage over prevailing diffusion-based purification models.

5.4. Influence on Clean Accuracy

To further assess the impact of PuriDefense on clean accuracy, we evaluate the performance decline for both CIFAR-10 and ImageNet datasets when utilizing all the standalone purification models implemented in DISCO and PuriDefense. Results in Figure 10 in Appendix G show that purification models illustrate comparable clean accuracy on low-resolution datasets, *i.e.* CIFAR-10, and achieves a higher clean accuracy on high-resolution datasets, *i.e.* ImageNet. We attribute this to the fact that natural image manifold exists in high-resolution datasets.

To test the influence of the number of the image patches on clean accuracy, we vary the number of patches ranging in $\{1 \times 1, 3 \times 3, 5 \times 5\}$ using ImageNet dataset. The results in Figure 11 in Appendix G shows that increasing the number of patches does not significantly affect the clean accuracy, PuriDefense achieves comparable clean accuracy to the case without any defense mechanism.

6. Conclusion

This paper introduces a novel theory-backed image purification mechanism utilizing local implicit function to defend deep neural networks against query-based adversarial attacks. The mechanism enhances classifier robustness and reduces successful attacks whilst also addressing vulnerabilities of deterministic transformations. Its effectiveness and robustness, which increase with the addition of purifiers, have been authenticated via extensive tests on CIFAR-10 and ImageNet. Our work highlights the need for dynamic and efficient defense mechanisms in MLaaS systems.

References

- Aithal, M. B. and Li, X. Boundary defense against black-box adversarial attacks. In *26th International Conference on Pattern Recognition, ICPR*. IEEE, 2022.
- Al-Dujaili, A. and O’Reilly, U. Sign bits are all you need for black-box attacks. In *8th International Conference on Learning Representations, (ICLR)*, 2020.
- Andriushchenko, M., Croce, F., Flammarion, N., and Hein, M. Square attack: A query-efficient black-box adversarial attack via random search. In *Computer Vision - (ECCV) - 16th European Conference*, Lecture Notes in Computer Science. Springer, 2020.
- Brendel, W., Rauber, J., and Bethge, M. Decision-based adversarial attacks: Reliable attacks against black-box machine learning models. In *6th International Conference on Learning Representations (ICLR)*, 2018.
- Cao, Y., Xiao, C., Cyr, B., Zhou, Y., Park, W., Rampazzi, S., Chen, Q. A., Fu, K., and Mao, Z. M. Adversarial sensor attack on lidar-based perception in autonomous driving. In *Proceedings of the 2019 ACM SIGSAC Conference on Computer and Communications Security, (CCS)*. ACM, 2019.
- Carlini, N. and Wagner, D. A. Towards evaluating the robustness of neural networks. In *2017 IEEE Symposium on Security and Privacy, (SP)*. IEEE Computer Society, 2017.
- Carlini, N., Tramèr, F., Dvijotham, K. D., Rice, L., Sun, M., and Kolter, J. Z. (certified!!) adversarial robustness for free! In *The Eleventh International Conference on Learning Representations, ICLR*, 2023.
- Chen, J., Jordan, M. I., and Wainwright, M. J. Hop-skipjumpattack: A query-efficient decision-based attack. In *2020 IEEE Symposium on Security and Privacy (SP) 2020*. IEEE, 2020.
- Chen, S., Huang, Z., Tao, Q., Wu, Y., Xie, C., and Huang, X. Adversarial attack on attackers: Post-process to mitigate black-box score-based query attacks. In *NeurIPS*, 2022.
- Chen, Y., Liu, S., and Wang, X. Learning continuous image representation with local implicit image function. In *IEEE Conference on Computer Vision and Pattern Recognition, (CVPR)*. Computer Vision Foundation / IEEE, 2021.
- Cheng, M., Le, T., Chen, P., Zhang, H., Yi, J., and Hsieh, C. Query-efficient hard-label black-box attack: An optimization-based approach. In *7th International Conference on Learning Representations (ICLR)*, 2019.
- Cheng, M., Singh, S., Chen, P. H., Chen, P., Liu, S., and Hsieh, C. Sign-opt: A query-efficient hard-label adversarial attack. In *8th International Conference on Learning Representations (ICLR)*, 2020.
- Clarifai, I. The generative developer platform. <https://www.clarifai.com/>, 2022. Accessed: 2023-09-25.
- Cohen, J., Rosenfeld, E., and Kolter, J. Z. Certified adversarial robustness via randomized smoothing. In *Proceedings of the 36th International Conference on Machine Learning, ICML*, Proceedings of Machine Learning Research. PMLR, 2019.
- Croce, F., Andriushchenko, M., Sehwag, V., DeBenedetti, E., Flammarion, N., Chiang, M., Mittal, P., and Hein, M. Robustbench: a standardized adversarial robustness benchmark. In *Proceedings of the Neural Information Processing Systems Track on Datasets and Benchmarks 1, (NeurIPS)*, 2021.
- Dadalto, E. Resnet18 trained on cifar10. https://huggingface.co/edadaltocg/resnet18_cifar10, 2022. Accessed: 2023-07-01.
- Deng, J., Dong, W., Socher, R., Li, L., Li, K., and Fei-Fei, L. Imagenet: A large-scale hierarchical image database. In *Computer Vision and Pattern Recognition (CVPR)*, 2009.
- Dong, Y., Su, H., Wu, B., Li, Z., Liu, W., Zhang, T., and Zhu, J. Efficient decision-based black-box adversarial attacks on face recognition. In *IEEE Conference on Computer Vision and Pattern Recognition, (CVPR)*. Computer Vision Foundation / IEEE, 2019.
- Goodfellow, I. J., Shlens, J., and Szegedy, C. Explaining and harnessing adversarial examples. In *3rd International Conference on Learning Representations, (ICLR)*, 2015.
- Google. Visual ai. <https://cloud.google.com/vision>, 2022. Accessed: 2023-09-25.
- Gowal, S., Qin, C., Uesato, J., Mann, T. A., and Kohli, P. Uncovering the limits of adversarial training against norm-bounded adversarial examples. *CoRR*, 2020.
- Guo, C., Gardner, J. R., You, Y., Wilson, A. G., and Weinberger, K. Q. Simple black-box adversarial attacks. In *Proceedings of the 36th International Conference on Machine Learning, (ICML)*, Proceedings of Machine Learning Research. PMLR, 2019.
- He, K., Zhang, X., Ren, S., and Sun, J. Deep residual learning for image recognition. In *Computer Vision and Pattern Recognition (CVPR)*, 2016.
- Ho, C. and Vasconcelos, N. DISCO: adversarial defense with local implicit functions. In *NeurIPS*, 2022.

- Ilyas, A., Engstrom, L., Athalye, A., and Lin, J. Black-box adversarial attacks with limited queries and information. In *Proceedings of the 35th International Conference on Machine Learning, (ICML)*. PMLR, 2018.
- Krizhevsky, A. Learning Multiple Layers of Features from Tiny Images. Technical report, Univ. Toronto, 2009.
- Kurakin, A., Goodfellow, I. J., and Bengio, S. Adversarial machine learning at scale. In *International Conference on Learning Representations (ICLR)*, 2017a.
- Kurakin, A., Goodfellow, I. J., and Bengio, S. Adversarial examples in the physical world. In *5th International Conference on Learning Representations, (ICLR), Workshop Track Proceedings*. OpenReview.net, 2017b.
- Lim, B., Son, S., Kim, H., Nah, S., and Lee, K. M. Enhanced deep residual networks for single image super-resolution. In *2017 IEEE Conference on Computer Vision and Pattern Recognition Workshops, (CVPR) Workshops*. IEEE Computer Society, 2017.
- Liu, S., Chen, P., Chen, X., and Hong, M. signsgd via zeroth-order oracle. In *7th International Conference on Learning Representations, (ICLR)*, 2019.
- Liu, X., Cheng, M., Zhang, H., and Hsieh, C. Towards robust neural networks via random self-ensemble. In *Computer Vision - ECCV 2018 - 15th European Conference*, Lecture Notes in Computer Science. Springer, 2018.
- Liu, Y., Chen, X., Liu, C., and Song, D. Delving into transferable adversarial examples and black-box attacks. In *5th International Conference on Learning Representations, (ICLR)*. OpenReview.net, 2017.
- Madry, A., Makelov, A., Schmidt, L., Tsipras, D., and Vladu, A. Towards deep learning models resistant to adversarial attacks. In *6th International Conference on Learning Representations, (ICLR)*. OpenReview.net, 2018.
- Mao, C., Chiquier, M., Wang, H., Yang, J., and Vondrick, C. Adversarial attacks are reversible with natural supervision. In *2021 IEEE/CVF International Conference on Computer Vision, (ICCV)*. IEEE, 2021.
- Nesterov, Y. E. and Spokoiny, V. G. Random gradient-free minimization of convex functions. *Found. Comput. Math.*, 2017.
- Nicolae, M.-I., Sinn, M., Tran, M. N., Buesser, B., Rawat, A., Wistuba, M., Zantedeschi, V., Baracaldo, N., Chen, B., Ludwig, H., Molloy, I., and Edwards, B. Adversarial robustness toolbox v1.2.0. *CoRR*, 2018.
- Nie, W., Guo, B., Huang, Y., Xiao, C., Vahdat, A., and Anandkumar, A. Diffusion models for adversarial purification. In *International Conference on Machine Learning, (ICML)*. Proceedings of Machine Learning Research. PMLR, 2022.
- Papernot, N. and McDaniel, P. D. On the effectiveness of defensive distillation. *CoRR*, 2016.
- Qin, Z., Fan, Y., Zha, H., and Wu, B. Random noise defense against query-based black-box attacks. In *Advances in Neural Information Processing Systems 34: Annual Conference on Neural Information Processing Systems 2021, NeurIPS 2021, December 6-14, 2021, virtual*, 2021.
- Raff, E., Sylvester, J., Forsyth, S., and McLean, M. Barrage of random transforms for adversarially robust defense. In *IEEE Conference on Computer Vision and Pattern Recognition, (CVPR)*. Computer Vision Foundation / IEEE, 2019.
- Rauber, J., Zimmermann, R., Bethge, M., and Brendel, W. Foolbox native: Fast adversarial attacks to benchmark the robustness of machine learning models in pytorch, tensorflow, and jax. *Journal of Open Source Software*, 2020.
- Salman, H., Ilyas, A., Engstrom, L., Kapoor, A., and Madry, A. Do adversarially robust imagenet models transfer better? In *Advances in Neural Information Processing Systems 33: Annual Conference on Neural Information Processing Systems 2020, (NeurIPS)*, 2020a.
- Salman, H., Sun, M., Yang, G., Kapoor, A., and Kolter, J. Z. Denoised smoothing: A provable defense for pretrained classifiers. In *Advances in Neural Information Processing Systems 33: Annual Conference on Neural Information Processing Systems 2020, NeurIPS*, 2020b.
- Sitawarin, C., Golan-Strieb, Z. J., and Wagner, D. A. Demystifying the adversarial robustness of random transformation defenses. In *International Conference on Machine Learning, ICML*, Proceedings of Machine Learning Research. PMLR, 2022.
- Szegedy, C., Zaremba, W., Sutskever, I., Bruna, J., Erhan, D., Goodfellow, I. J., and Fergus, R. Intriguing properties of neural networks. In *2nd International Conference on Learning Representations (ICLR)*, 2014.
- Torchvision. Resnet50 - torchvision main documentation. <https://pytorch.org/vision/main/models/generated/torchvision.models.resnet50.html>, 2023. Accessed: 2023-11-11.
- Tramèr, F., Kurakin, A., Papernot, N., Goodfellow, I. J., Boneh, D., and McDaniel, P. D. Ensemble adversarial training: Attacks and defenses. In *6th International Conference on Learning Representations (ICLR)*, 2018.

- VentureBeat. Facebook user data: 845m monthly users, 2.7b daily likes & comments. <https://venturebeat.com/business/facebook-ipo-usage-data/>, 2022. Accessed: 2023-09-25.
- Xu, W., Evans, D., and Qi, Y. Feature squeezing: Detecting adversarial examples in deep neural networks. In *25th Annual Network and Distributed System Security Symposium, NDSS*. The Internet Society, 2018.
- Yang, G., Duan, T., Hu, J. E., Salman, H., Razenshteyn, I. P., and Li, J. Randomized smoothing of all shapes and sizes. In *Proceedings of the 37th International Conference on Machine Learning, (ICML)*, Proceedings of Machine Learning Research. PMLR, 2020.
- Yoon, J., Hwang, S. J., and Lee, J. Adversarial purification with score-based generative models. In *Proceedings of the 38th International Conference on Machine Learning, (ICML)*. PMLR, 2021.
- Zagoruyko, S. and Komodakis, N. Wide residual networks. In *Proceedings of the British Machine Vision Conference 2016, (BMVC)*, 2016.
- Zhang, Y., Li, K., Li, K., Wang, L., Zhong, B., and Fu, Y. Image super-resolution using very deep residual channel attention networks. In *Computer Vision - ECCV 2018 - 15th European Conference*, Lecture Notes in Computer Science. Springer, 2018.

A. Background for General Defense

More on General Defense for Query-based Attacks The defense for black-box query-based attacks remain relatively unexplored compared to the defense for white-box methods (Qin et al., 2021). Under considerations of real-world constraints such as clean accuracy and inference speed, most training-time and testing-time defenses present significant limitations for deployment in real-world MLaaS systems. For training-time defense, the aim is to improve the worst-case robustness of the models. Adversarial training (AT) has been considered as one of the fundamental practices of training time defense, where models are trained on augmented datasets with specially-crafted samples to ensure robustness of the models (Madry et al., 2018). Other training-time examples like gradient masking (Tramèr et al., 2018) and defensive distillation (Papernot & McDaniel, 2016) are also proposed to improve the robustness of the models. Nonetheless, such methods are unsuitable for MLaaS systems because of the extensive training costs and potential for decreased accuracy on clean examples. With regards to testing-time defense, a prominent defense from white-box attacks, randomized smoothing, can ensure the robustness of the model within a certain confidence level (Yang et al., 2020), a feature known as certified robustness. Another example for multiple inference to improve the robustness is called random self-ensemble (Liu et al., 2018). However, the inference speed of randomized smoothing is too slow to be deployed on real-world MLaaS systems. Other testing-time defenses tend towards randomization of the input or output. Rand noise defense proposed by Qin et al. (2021) leverages Gaussian noises as the input to the model to disturb the gradient estimation. Yet, the defense is ineffective against strong attack methods and hurts the clean accuracy. The output-based defense, like confidence poisoning (Chen et al., 2022) influences the examples on the classification boundary and cannot defend against the decision-based attacks.

B. Search Techniques for black-box attacks

Projected Gradient Descent A common approach of performing adversarial attacks (often white-box) is to leverage projected gradient descent algorithm (Carlini & Wagner, 2017):

$$\mathbf{x}_{t+1} = Proj_{N_R(\mathbf{x})}(\mathbf{x} - \eta_t g(\mathbf{x})_t). \quad (10)$$

Gradient Estimation While there can be various gradient estimators, we consider the following gradient estimator in our theoretical analysis:

$$g(\mathbf{x}) = \frac{f(\mathbf{x} + \mu \mathbf{u}) - f(\mathbf{x})}{\mu} \mathbf{u}. \quad (11)$$

Heuristic Search For heuristic search, the main issue is to determine the search direction. One commonly used search direction can be:

$$s(\mathbf{x}) = \mathbb{I}(h(\mathbf{x}) < 0) \cdot \mu \mathbf{u}, \quad \text{where } h(\mathbf{x}) = f(\mathbf{x} + \mu \mathbf{u}) - f(\mathbf{x}), \quad (12)$$

where \mathbb{I} is the indicator function. The search direction is determined by the sign of the objective function. If the objective function is negative, the search direction is the gradient direction. Otherwise, the search direction is the opposite of the gradient direction. The corresponding updating direction will be Equation (10) with $-\eta_t g(\mathbf{x})_t$ replaced by $s(\mathbf{x}_t)$.

C. Details for Experiments

C.1. Comparison of the Inference Speed on ImageNet Dataset

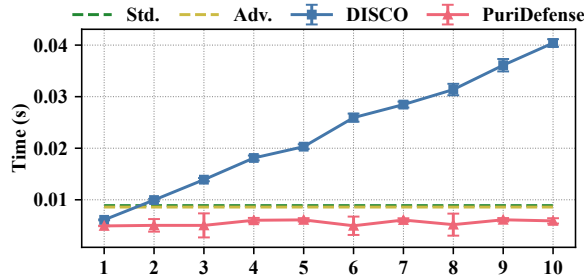


Figure 8. The inference speed of DISCO and PuriDefense on ImageNet dataset.

C.2. Details of the Attacks

We utilize 5 SOTA query-based attacks for evaluation: NES (Ilyas et al., 2018), SimBA (Guo et al., 2019), Square (Andriushchenko et al., 2020), Boundary (Brendel et al., 2018), and HopSkipJump (Chen et al., 2020). The category of them is listed below in Table 3.

Table 3. The category of the attacks along with the techniques they use.

	Gradient Estimation	Random Search
Score-based	NES	Square, SimBA
Decision-based	Boundary	HopSkipJump

Implementation For Boundary Attack and HopSkipJump Attack, we adopt the implementation from Foolbox (Rauber et al., 2020). For Square Attack and SimBA, we use the implementation from ART library (Nicolae et al., 2018). For NES, we implement it under the framework of Foolbox.

Hyperparameters The hyperparameters used for the attacks are listed below for full reproducibility.

Table 4. The hyperparameters used for NES.

	CIFAR-10	ImageNet
η (learning rate)	0.01	0.0005
q (number of points used for estimation)	100	100

Table 5. The hyperparameters used for SimBA.

	CIFAR-10	ImageNet
η (step size)	0.2	0.2

Table 6. The hyperparameters used for Square.

	CIFAR-10	ImageNet
μ (Fraction of Pixel Changed)	0.05 ~ 0.5	0.05 ~ 0.5

Table 7. The hyperparameters used for Boundary Attack.

	CIFAR-10	ImageNet
η_{sph} (Spherical Step)	0.01	0.01
η_{src} (Source Step)	0.01	0.01
η_c (Source Step Converge)	1E-7	1E-7
η_a (Step Adaptation)	1.5	1.5

Table 8. The hyperparameters used for HopSkipJump Attack.

	CIFAR-10	ImageNet
n (number for estimation)	100	100
γ (Step Control Factor)	1	1

C.3. Detailed Information for the Defense

We compare our algorithm with three types of baseline defense. For random noise defense, we use a Gaussian noise with $\sigma = 0.041$ as the input to the classifier. For the spatial smoothing transformations, we set the size of the kernel filter to be 3. For DISCO model, we implement a naive version without randomness using pre-trained models from the official implementation. We pick the pre-trained model under PGD attack (Madry et al., 2018) as the core local implicit model for DISCO.

C.4. Testing models.

We use the WideResNet-28-10 (Zagoruyko & Komodakis, 2016) achieving a 94.78% accuracy rate for CIFAR-10, and ResNet-50 (He et al., 2016) with 76.52% accuracy for ImageNet for the standardly trained models. For models trained adversarially, we use the WideResNet-28-10 model with 89.48% adversarial accuracy trained by Gowal et al. (2020) for CIFAR-10 and ResNet-50 model with 64.02% trained by Salman et al. (2020a) for ImageNet.

D. Details for PuriDefense

D.1. Efficient Structure for Inference Speed Up

Upon examining the implementation of the local implicit function as outlined by (Chen et al., 2021), it became apparent that the local ensemble mechanism geared toward enhancing performance in super-resolution tasks is unnecessary for the

adversarial purification process. Refer to Figure 9 for a conceptual depiction of the previously utilized technique.

Given that image purification requires direct one-to-one pixel correspondence, the act of inferring the same pixel multiple times before averaging the outcomes is redundant. Consequently, discarding this mechanism simplifies the approach to using the local implicit function solely for image purification. This adjustment accelerates the inference speed of the original implementation of local implicit models by a factor of four.

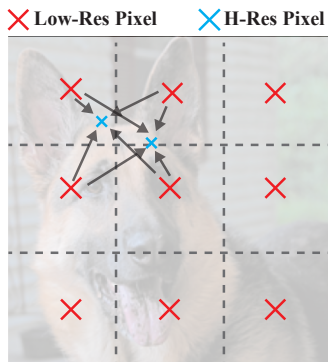


Figure 9. An illustration of the local ensemble mechanism in the local implicit function for multi-resolution support. High resolution pixels are predicted based on high-level features from nearby low resolution pixels.

D.2. Training Diversified Purifiers

For improving the diversity of the purifiers, we consider the following influence factors in Table 9 and use their combinations to train 12 different purification models for each dataset.

Non-defended Models. For CIFAR-10, we use a pre-trained ResNet-18 model (Dadalto, 2022) for generating adversarial examples under white-box attacks. For ImageNet, we use a pre-trained ResNet-50 model (Torchvision, 2023) for generating adversarial examples. We list these models along with their clean accuracy on the test set in Table 10.

Training Datasets. For CIFAR-10, we use the whole training set of CIFAR-10 to train the purifiers. While for datasets containing natural images, using only a subset of the training set can help the purification model learn the natural image. Thus, for ImageNet dataset, we randomly sampled 10 images from each class of the original training set to form a new training set for training the purifiers.

Table 9. The factors that are considered when training diversified purification models for PuriDefense.

Hyperparameter	Value
Attack Type	FGSM (Goodfellow et al., 2015)
	PGD (Madry et al., 2018)
	BIM (Kurakin et al., 2017a)
Encoder Structure	RCAN (Zhang et al., 2018)
	EDSR (Lim et al., 2017)
Feature Depth	32, 64

Table 10. The non-defended models used to generate adversarial examples.

Model Structure	Dataset	Clean Accuracy
ResNet-18 (Dadalto, 2022)	CIFAR-10	94.8%
ResNet-50 (Torchvision, 2023)	ImageNet	80.9%

E. Supplementary Materials for Theoretical Analysis

E.1. Important Definitions

Definition 1. The Gaussian-Smoothing function corresponding to $f(\mathbf{x})$ with $\mu > 0$, $\mathbf{u} \sim \mathcal{N}(\mathbf{0}, \mathbf{I})$ is

$$f_\mu(\mathbf{x}) = \frac{1}{(2\pi)^{d/2}} \int f(\mathbf{x} + \mu\mathbf{u}) e^{-\frac{\|\mathbf{u}\|^2}{2}} d\mathbf{u} \quad (13)$$

E.2. Proof of Theorem 1

The essential lemmas are given as follows, the complete proofs are shown in (Nesterov & Spokoiny, 2017).

Lemma 1. Let $f(\mathbf{x})$ be the Lipschitz-continuous function, $|f(\mathbf{y}) - f(\mathbf{x})| \leq L_0(f)\|\mathbf{y} - \mathbf{x}\|$. Then

$$L_1(f_\mu) = \frac{d^{\frac{1}{2}}}{\mu} L_0(f)$$

We define the p -order moment of normal distribution as M_p . Then we have

Lemma 2. For $p \in [0, 2]$, we have

$$M_p \leq d^{\frac{p}{2}}$$

If $p \geq 2$, then we have two-side bounds

$$d^{\frac{p}{2}} \leq M_p \leq (p + d)^{\frac{p}{2}}$$

Lemma 3. Let $f(\mathbf{x})$ be the Lipschitz-continuous function, $|f(\mathbf{y}) - f(\mathbf{x})| \leq L_0(f)\|\mathbf{y} - \mathbf{x}\|$. And $\mathbf{m}(\mathbf{x})$ is Lipschitz-continuous for every dimension. Then

$$L_0(f \circ \mathbf{m}) \leq L_0(f)L_0(\mathbf{m})$$

where $L_0(\mathbf{m})$ is defined as $L_0(\mathbf{m}) = \max_i L_0(m_i)$.

Proof.

$$\begin{aligned} |f(\mathbf{m}(\mathbf{y})) - f(\mathbf{m}(\mathbf{x}))| &\leq L_0(f)\|\mathbf{m}(\mathbf{y}) - \mathbf{m}(\mathbf{x})\| \\ &= L_0(f) \sqrt{\sum_{i=1}^d L_0(\mathbf{m}_i)^2 (\mathbf{y}_i - \mathbf{x}_i)^2} \\ &\leq L_0(f)L_0(\mathbf{m})\|\mathbf{y} - \mathbf{x}\| \end{aligned} \quad (14)$$

□

The following content is the proof for Theorem 1.

Proof. According to the property of Lipschitz-continuous gradient,

$$F_{\mu,K}(\mathbf{x}_{t+1}) \leq F_{\mu,K}(\mathbf{x}_t) - \eta_t \langle \nabla F_{\mu,K}(\mathbf{x}_t), G_{\mu,K}(\mathbf{x}_t) \rangle + \frac{1}{2} \eta_t^2 L_1(F_{\mu,K}) \|G_{\mu,K}(\mathbf{x}_t)\|^2 \quad (15)$$

The $G_{\mu,K}(\mathbf{x}_t)$ can be decomposed as

$$\begin{aligned} G_{\mu,K}(\mathbf{x}_t) &= \frac{f(\mathbf{m}_{k_{t1}}(\mathbf{x} + \mu\mathbf{u})) - f(\mathbf{m}_{k_{t2}}(\mathbf{x}))}{\mu} \mathbf{u}_t \\ &= \frac{f(\mathbf{m}_{k_{t1}}(\mathbf{x} + \mu\mathbf{u})) - f(\mathbf{m}_0(\mathbf{x} + \mu\mathbf{u})) + f(\mathbf{m}_0(\mathbf{x} + \mu\mathbf{u})) - f(\mathbf{m}_0(\mathbf{x}))}{\mu} \mathbf{u}_t \\ &\quad + \frac{f(\mathbf{m}_0(\mathbf{x})) - f(\mathbf{m}_{k_{t2}}(\mathbf{x}))}{\mu} \mathbf{u}_t \end{aligned} \quad (16)$$

The squared term $\|G_{\mu,K}(\mathbf{x}_t)\|^2$ is bounded by

$$\|G_{\mu,K}(\mathbf{x}_t)\|^2 \leq \frac{4\nu^2}{\mu^2} L_0(f)^2 \|\mathbf{u}_t\|^2 + \frac{4\nu}{\mu} L_0(F)L_0(f) \|\mathbf{u}_t\|^3 + L_0(F)^2 \|\mathbf{u}_t\|^4 \quad (17)$$

Take the expectation over \mathbf{u}_t , k_{t1} , and k_{t2} , use Lemma 2, we have

$$\begin{aligned} F_{\mu,K}(\mathbf{x}_{t+1}) &\leq F_{\mu,K}(\mathbf{x}_t) - \eta_t \|\nabla F_{\mu,K}(\mathbf{x}_t)\|^2 \\ &\quad + \frac{1}{2} \eta_t^2 L_1(F_{\mu,K}) \left(\frac{4\nu^2}{\mu^2} L_0(f)^2 d + \frac{4\nu}{\mu} L_0(F) L_0(f) (d+3)^{\frac{3}{2}} + L_0(F)^2 (d+4)^2 \right) \end{aligned} \quad (18)$$

For $L_1(F_{\mu,K})$, we have:

$$L_1(F_{\mu,K}) = \frac{1}{K} \sum_{k=1}^K L_1(f_{\mu}(\mathbf{m}_k)) \leq \frac{L_0(F) d^{\frac{1}{2}}}{\mu} \quad (19)$$

Use Lemma 1, and the dimension d is high, we have

$$\begin{aligned} F_{\mu,K}(\mathbf{x}_{t+1}) &\leq F_{\mu,K}(\mathbf{x}_t) - \eta_t \|\nabla F_{\mu,K}(\mathbf{x}_t)\|^2 \\ &\quad + \frac{1}{2} \eta_t^2 \frac{L_0(f)^3 L_0(\mathbf{m}_0) d^{\frac{3}{2}}}{\mu} \left(\frac{4\nu^2}{\mu^2} + \frac{4\nu}{\mu} L_0(\mathbf{m}_0) d^{\frac{1}{2}} + L_0(\mathbf{m}_0)^2 d \right) \end{aligned} \quad (20)$$

We take the expectation over $\mathbf{U}_t, \mathbf{k}_t$.

$$\begin{aligned} \mathbb{E}_{\mathbf{U}_t, \mathbf{k}_t} [F_{\mu,K}(\mathbf{x}_{t+1})] &\leq \mathbb{E}_{\mathbf{U}_{t-1}, \mathbf{k}_{t-1}} [F_{\mu,K}(\mathbf{x}_t)] - \eta_t \mathbb{E}_{\mathbf{U}_t, \mathbf{k}_t} [\|\nabla F_{\mu,K}(\mathbf{x}_t)\|^2] \\ &\quad + \frac{1}{2} \eta_t^2 \frac{L_0(f)^3 L_0(\mathbf{m}_0) d^{\frac{3}{2}}}{\mu} \left(\frac{4\nu^2}{\mu^2} + \frac{4\nu}{\mu} L_0(\mathbf{m}_0) d^{\frac{1}{2}} + L_0(\mathbf{m}_0)^2 d \right) \end{aligned} \quad (21)$$

Now consider constant step size $\eta_t = \eta$, and sum over t from 0 to Q , we have

$$\begin{aligned} \frac{1}{Q+1} \sum_{t=0}^Q \mathbb{E}_{\mathbf{U}_t} [\|\nabla F_{\mu,K}(\mathbf{x}_t)\|^2] &\leq \frac{1}{\eta} \left(\frac{F_{\mu,K}(\mathbf{x}_0) - F_K^*}{Q+1} \right) \\ &\quad + \frac{1}{2} \eta \frac{L_0(f)^3 L_0(\mathbf{m}_0) d^{\frac{3}{2}}}{\mu} \left(\frac{4\nu^2}{\mu^2} + \frac{4\nu}{\mu} L_0(\mathbf{m}_0) d^{\frac{1}{2}} + L_0(\mathbf{m}_0)^2 d \right) \end{aligned} \quad (22)$$

Since the distance between the input variable should be bounded by R and use Lipschitz-continuous, we have

$$\|F_{\mu,K}(\mathbf{x}_0) - F_K^*\| \leq \frac{1}{K} L_0(f) \sum_{k=0}^K L_0(\mathbf{m}_k) R \leq L_0(F) R \quad (23)$$

Considering bounded $\mu \leq \hat{\mu} = \frac{\epsilon}{d^{\frac{1}{2}} L_0(F)}$ to ensure local Lipschitz-continuity, and set $\gamma(\mathbf{m}_0, \nu) = \frac{4\nu^2}{\mu^2} + \frac{4\nu}{\mu} L_0(\mathbf{m}_0) d^{\frac{1}{2}} + L_0(\mathbf{m}_0)^2 d$

$$\frac{1}{Q+1} \sum_{t=0}^Q \mathbb{E}_{\mathbf{U}_t, \mathbf{k}_t} [\|\nabla F_{\mu}(\mathbf{x}_t)\|^2] \leq \frac{1}{\eta} \left(\frac{L_0(F) R}{Q+1} \right) + \frac{1}{2} \eta \frac{L_0(f)^4 L_0(\mathbf{m}_0)^2}{\epsilon} d^2 \gamma(\mathbf{m}_0, \nu) \quad (24)$$

Minimize the right hand size,

$$\eta = \sqrt{\frac{2R\epsilon}{(Q+1)L_0(f)^3 d^2}} \cdot \sqrt{\frac{1}{L_0(\mathbf{m}_0) \gamma(\mathbf{m}_0, \nu)}} \quad (25)$$

And we get

$$\frac{1}{Q+1} \sum_{t=0}^Q \mathbb{E}_{\mathbf{U}_t, \mathbf{k}_t} [\|\nabla F_{\mu}(\mathbf{x}_t)\|^2] \leq \sqrt{\frac{2L_0(f)^5 R d^2}{(Q+1)\epsilon}} \cdot \sqrt{\gamma(\mathbf{m}_0, \nu) L_0(\mathbf{m}_0)^3} \quad (26)$$

To guarantee the expected squared norm of the gradient of function F_{μ} of the order δ , the lower bound for the expected number of queries is

$$O\left(\frac{L_0(f)^5 R d^2}{\epsilon \delta^2} \gamma(\mathbf{m}_0, \nu) L_0(\mathbf{m}_0)^3\right) \quad (27)$$

□

E.3. Proof of Theorem 2

Proof.

$$\begin{aligned}
 P(\text{Sign}(H(\mathbf{x})) \neq \text{Sign}(H_K(\mathbf{x}))) &\leq P(|H_K(\mathbf{x}) - H(\mathbf{x})| \geq |H(\mathbf{x})|) \\
 &\leq \frac{\mathbb{E}[|H_K(\mathbf{x}) - H(\mathbf{x})|]}{|H(\mathbf{x})|} \\
 &\leq \frac{\sqrt{\mathbb{E}[(H_K(\mathbf{x}) - H(\mathbf{x}))^2]}}{|H(\mathbf{x})|} \\
 &\leq \frac{\sqrt{\mathbb{E}[2(f(\mathbf{m}_{k_1}(\mathbf{x} + \mu\mathbf{u})) - f(\mathbf{m}_0(\mathbf{x} + \mu\mathbf{u})))^2 + 2(f(\mathbf{m}_{k_2}(\mathbf{x})) - f(\mathbf{m}_0(\mathbf{x})))^2]}}{|H(\mathbf{x})|} \\
 &\leq \frac{2\nu L_0(f)}{|H(\mathbf{x})|}
 \end{aligned} \tag{28}$$

F. Accuracy for ImageNet

Table 11. Evaluation results of PuriDefense and other defense methods on ImageNet under 5 SOTA query-based attacks. The robust accuracy under 200/2500 queries is reported. The best defense mechanism under 2500 queries are highlighted in bold and marked with gray.

Datasets	Methods	Acc.	NES(ℓ_∞)	SimBA(ℓ_2)	Square(ℓ_∞)	Boundary(ℓ_2)	HopSkipJump(ℓ_∞)
ImageNet (ResNet-50)	None	76.5	72.9/61.2	65.5/50.8	37.6/5.2	70.7/64.9	68.3/66.0
	AT (Gowal et al., 2020)	57.5	52.2/51.1	54.5/50.7	52.9/46.8	57.1/57.0	57.5/57.3
	FS (Xu et al., 2018)	68.2	71.5/59.4	61.4/28.2	28.8/2.3	66.5/60.4	64.4/64.4
	IR (Qin et al., 2021)	64.7	64.0/63.0	61.7/58.3	62.3/60.1	65.3/64.9	64.8/65.5
	DISCO (Ho & Vasconcelos, 2022)	67.7	65.9/60.9	61.0/25.7	34.5/5.1	65.9/63.3	67.0/64.6
	PuriDefense (Ours)	66.7	65.5/62.9	63.1/61.3	65.0/59.1	66.6/65.3	66.2/66.0
	PuriDefense-AT (Ours)	57.8	56.0/54.7	54.0/53.5	55.4/53.2	56.8/57.1	56.8/56.1

G. Influence on Clean Accuracy

One of the biggest advantage of local implicit purification is that it does not affect the clean accuracy of the model. While the results for evaluation of our mechanism’s robust accuracy are shown in Table 2 in section 5, we also provide the results for clean accuracy in figure 10. Moreover, we have conducted extra experiments on the influence of the numbers of the image patches on the clean accuracy. The results are shown in figure 11. The results are obtained using the whole test set of CIFAR-10 and validation set of ImageNet.

Comaprison of Defense Mechanisms. We first test clean accuracy on each purification model contained in DISCO and our method. The label name refers to the white-box attacks used to generate adversarial examples for training the purification model. For PuriDefense, a list of the purification model and their according attack and encoder combination can be found in Table 12. For both datasets, all the purification models have a better clean accuracy than adding random noise. Moreover, they all achieve better clean accuracy than adversarially trained models on ImageNet dataset.

Influence of the Number of Patches. We then test the influence of the number of patches on the clean accuracy. In PuriDefense, we only use image patches for feature encoding and purification. Therefore, the number of patches is a hyperparameter that can be tuned. We test the influence of the number of patches on the clean accuracy. The results are shown in figure 11. We can see that the clean accuracy is not affected by the number of patches.

Table 12. The purification model used in PuriDefense.

Model Type	p0	p1	p2	p3	p4	p5
Attack Encoder	BIM_EDSR	BIM_RCAN	FGSM_EDSR	FGSM_RCAN	PGD_EDSR	PGD_RCAN

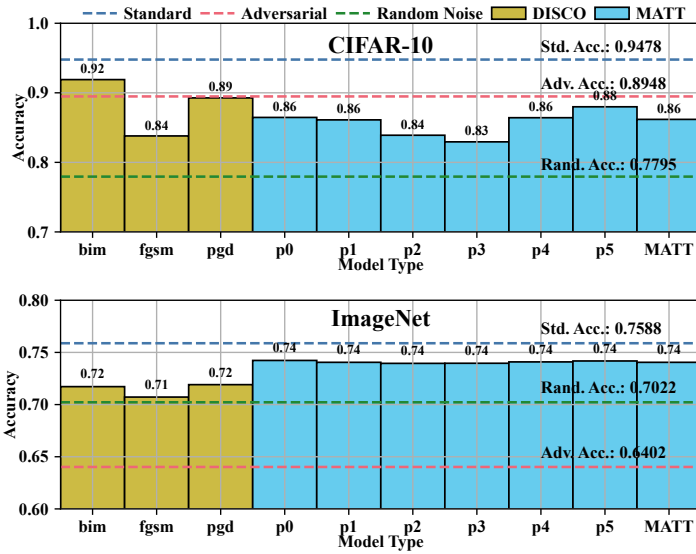


Figure 10. Comparison of defense mechanisms and models on clean accuracy. **Upper Figure:** CIFAR-10 dataset. **Lower Figure:** ImageNet dataset.

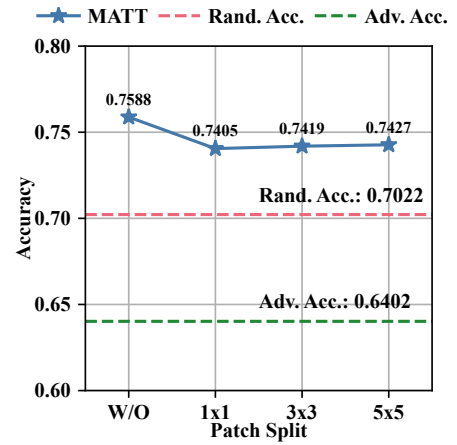


Figure 11. Influence of the number of image patches in PuriDefense.